DELIVERABLE REPORT

Deliverable no. / title:	4.1 / Single Cell Performance Model
Lead beneficiary:	ZHAW
Nature of deliverable:	Report & Open-Source Software
Dissemination level:	PU – Public, fully open, e.g. web
Due date:	M1 / January 2020

Grant Agreement number:	875489
Project acronym:	SONAR
Project title:	Modelling for the search for new active materials for redox flow batteries
Funding scheme:	H2020-LC-BAT-2019
Coordinator:	Fraunhofer ICT Jens Noack **Tel:** 0049 721 4640 870 **E-mail:** jens.noack@ict.fraunhofer.de
Project website:	www.sonar-redox.eu

Contents

Table of Symbols

Symbol	Description	Unit
$a_{\alpha,k}$	Activity of species α in compartment k	–
a_s	Specific electrode surface area	m^{-1}
A_{mem}	Total membrane area ($A_{\mathrm{mem}} = L_w L_h$)	m^2
A_s	Total electrode surface area	m^2
$b_{\alpha,k}$	Molality of species α in compartment k	$\mathrm{mol\,kg}^{-1}$
$c_{\alpha,k}$	Molar concentration of species α in compartment k	$\mathrm{mol\,L}^{-1}$
$D_{\alpha,k}$	Diffusion coefficient of species α in compartment k	$\mathrm{m}^2\mathrm{s}^{-1}$
i_k	Electric current density in compartment k	$\mathrm{A\,m}^{-2}$
$i_{0,k}$	Exchange current density in compartment k	$\mathrm{A\,m}^{-2}$
i_{mem}	Electric current density (I/A_{mem})	$\mathrm{A\,m}^{-2}$
I	Total electric current	A
$s_{q,k}$	Volumetric rate of charge production in compartment k	$\mathrm{A\,m}^{-3}$
$n_{\alpha,k}$	Number of moles of species α in compartment k	mol
f	Inverse thermal voltage ($f = F/(RT)$)	V^{-1}
F	Faraday constant	$\mathrm{C\,mol}^{-1}$
L_{el}	Thickness of electrode compartment (in through-plane direction)	m
L_m	Thickness of the membrane (in through-plane direction)	m
L_h	Height of the electrochemical cell	m
L_w	Width of the electrochemical cell	m
$\boldsymbol{n}$	Normal vector	–
Q	Total available charge	Ah
Q_F	Volumetric flow rate in compartment	$\mathrm{m}^3\mathrm{s}^{-1}$
SoC	State of charge of the battery	–
t_α	Transport number of species α	–
T	Temperature	K
V_{el}	Total electrode compartment volume ($V_{\mathrm{el}} = L_{el} L_w L_h$)	m^3
$V_{m,\alpha}$	Molar volume of species α	$\mathrm{L\,mol}^{-1}$
v_s	Superficial velocity	$\mathrm{m\,s}^{-1}$
Greek symbols	**Description**	**Unit**
α_k	Butler-Volmer symmetry coefficient in electrode compartment k	–
$\gamma_{\alpha,k}$	Activity coefficient of species α in compartment k	–
$\Delta\phi_{\mathrm{eq},k}$	Half-cell equilibrium potential in electrode compartment k	V
ε_p	Porosity of the electrode	–
η_k^{BV}	Total Butler-Volmer overpotential in compartment k	V
$\kappa_{d,\alpha}$	Electro-osmotic drag coefficient of species α	–
$\kappa_{s,\alpha}$	Solvation shell of species α	–
Λ_c	Model validity parameter indicating relative concentration variations	–
μ_α	Chemical potential of species α	$\mathrm{J\,kg}^{-1}$

Table 1: List of symbols used in the report.

1 Introduction

The rise of carbon-neutral energy systems, such as wind and solar energy systems, has increased the demand for local energy storage devices. Redox flow battery (RFB) systems are a promising technology for local energy storage. Since they allow an independent scaling of energy capacity and power, RFB systems can be readily adapted to the local energy grid requirements, see e.g. [8]. Aqueous organic based redox flow battery (AORFB) systems promise lower electrolyte costs and reduced environmental impact compared to metal-based electrolyte systems [6].

In this report we present a novel physics-based single-cell model for organic redox flow batteries, which we refer to as 0D-U-I-SoC model in the following. The model allows the performance prediction of single RFB cells by expressing the voltage and power density, in terms of the state of charge (SoC) and the electric current density. For illustration and validation purposes, we consider the application of the model to the organic TEMPTMA/MV electrolyte system [8]. However, the model presented in this report can be easily adapted to various electrolyte systems.

As shown by Sharma et al. [12], spatial variations of the electrolyte bulk composition in the electrode compartments can be neglected under typical operating conditions of RFB cells reported in the literature. Thus, within a specific window of operating conditions, the electrolyte bulk composition within each electrode compartment can be expressed in terms of average bulk quantities, which allows for a dimensionality reduction of the model to 0D.

The model takes into account important processes, such as the overpotentials resulting from the electron transfer at the electrode and concentration differences in the species concentrations at the electrode surface and the electrolyte bulk. In contrast to the dimensionality-reduced models by Murthy et al. [10] and Sharma et al. [12], the model considers the electro-osmotic cross effect, which leads to SoC dependent changes of the electrolyte volume. Furthermore, the model is formulated in terms of electrolyte activities, which allows taking into account non-ideal effects of concentrated electrolyte solutions.

Processes that occur over longer time scales, such as osmosis and degradation processes of the electrolyte and battery components are not considered, such that the model predictions are valid over time scales that are much shorter than the time-scales of the degradation processes. Neglecting these irreversible processes allows to establish a simple functional relationship between the SoC and the electrolyte bulk composition. Furthermore, the electrolyte concentrations at the electrode surface can be expressed in terms of the electrolyte bulk concentrations and the local electric current density. Ultimately, these relations allow expressing the cell voltage in terms of SoC and electric current density.

The 0D-U-I-SoC model presented in this report has been implemented in Mathematica 12 and published as open-source software under the 3-clause BSD license, which also permits the commercial use. The software is maintained on the GitHub account *ISOMORPH-Electrochemical Cells*, from where it can be

obtained. The open-source model implementation can serve as a point of departure for modelling and simulation of organic redox flow batteries in academic research and industry.

After introducing the cell geometry and the main model assumptions in Section 2 we discuss the considered electrolyte solutions, the redox reactions and introduce the TEMPTMA/MV electrolyte system in Sections 3-5.

We then consider a battery voltage model, which expresses the overall cell potential as the sum of the half-cell equilibrium potentials and the overpotentials based on the Butler-Volmer model in terms of electrolyte activities in Section 9. Restricting the symmetry coefficient in the Butler-Volmer model to $\alpha = 0.5$ allows for an explicit expression of the overpotential in terms of the current density. In Section 10 we introduce a simple transport model for the electroactive species in the diffusion layer around the carbon fibers, which allows the determination of the unknown surface concentrations in the derived overpotential expression. Section 12 presents an experimental validation of the 0D-U-I-SoC model with several cycling and polarization experiments for the TEMPTMA/MV electrolyte system. Finally, the main results are summarized and discussed in the concluding Section 13.

2 Model Geometry and Simplifying Assumptions

Figure 1 shows a simplified cell geometry of a single membrane electrode assembly (MEA) of a redox flow battery. The cell is composed of the negative electrode compartment, a membrane separating the electrode compartments, and a positive electrode compartment. The electrolyte flows through the porous electrodes in the vertical direction.

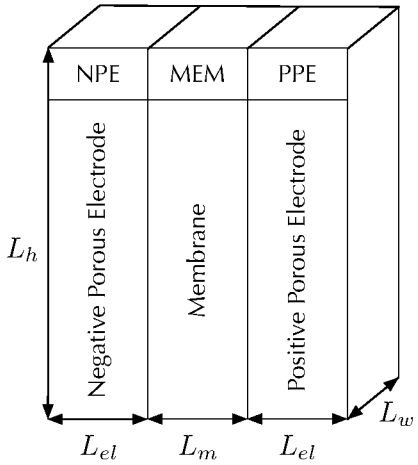

Figure 1: Cell Geometry

We are interested in predicting the overall cell voltage and power in terms of the applied electric current and state of charge for a range of typical operating

conditions over time scales that are much shorter than slow diffusion and osmosis fluxes through the membrane and irreversible degradation of the electrolyte material or cell components. Specifically, the main modelling assumptions are:

1. Spatial composition variations in the electrolyte bulk flow within each electrode compartment can be neglected,

2. The electric potential gradients in the metal electrode are small compared to the electric potential gradients through the MEA.

3. Degradation processes in cell components and electrolyte material are slow relative to the time-scale of observation.

4. The osmosis and diffusion processes through the membrane are negligible over the observed time-scale.

Clearly, these assumptions are only satisfied within a specific range of operating conditions and observation time scales. An analysis of the implied restriction on the magnitude of the applied current is shown by Murthy et al. [10].

3 Electrolyte Solution

Let us first consider the electrolyte solution within a single electrode compartment. The species in the electrolyte solution are denoted by $\mathscr{M}_\alpha$ for $\alpha = 0,\dots,N$, where $\mathscr{M}_0$ refers the solvent. Thus, the number of electrolyte species within each compartment is $N+1$. Both the solvent molecules and one ionic species, $\alpha^\star$, are necessarily present in both compartments. The latter species is transported by ionic migration through the membrane to satisfy macroscopic charge neutrality within each electrode compartment. Due to the assumption of zero cross-over of electroactive material and diffusion of neutral solute components through the membrane, the composition of all other species is determined solely by the initial concentration and the electrochemical reactions in the electrodes.

In the following we use the compact notation $\mathscr{M}_{\alpha,\pm}$ to refer to species α_+ in the posolyte and species α_- in the negolyte. As described above, since both solvent and at least one ionic species $\alpha^\star$ are present in both electrode compartments we have $\mathscr{M}_{0,+} = \mathscr{M}_{0,-}$ and $\mathscr{M}_{\alpha^\star,+} = \mathscr{M}_{\alpha^\star,-}$.

The dissolved species $\mathscr{M}_{\alpha,\pm}$ are related to the neutral components $\mathscr{S}_{\alpha,\pm}$ by the dissociation reaction

$$\mathscr{S}_{\alpha,\pm} \leftrightharpoons \sum_\beta \nu_{\alpha\beta,\pm}\mathscr{M}_{\alpha,\pm}, \tag{1}$$

where $\nu_{\alpha\beta,\pm} \in \mathbb{N}_0$ are the Stoichiometric coefficients. The salts are assumed to be dissociated completely in the solution.

We assume the principle of strong electroneutrality to hold in the electrolyte solution, so that

$$\sum_{\alpha} z_{\alpha,\pm} c_{\alpha,\pm}(\boldsymbol{x}) = 0 \tag{2}$$

is satisfied at all positions $\boldsymbol{x}$ in the solution, where $z_{\alpha,\pm}$ is the charge number of $\mathscr{M}_{\alpha,\pm}$ and $c_{\alpha,\pm}$ denotes the molar concentration of $\mathscr{M}_{\alpha,\pm}$.

Let $n_{0,\pm}$ denote the number of moles of solvent in the positive and negative electrode compartments, respectively. Analogously, $n_{\alpha,\pm}$ for $\alpha = 1,\dots,N$ denote the number of moles of dissolved ionic species. The molal concentration of the solutes are then given by

$$b_{\alpha,\pm} = \frac{n_{\alpha,\pm}}{m_{0,\pm}}, \tag{3}$$

where $m_{0,\pm} = n_{0,\pm} M_0$ denotes the total mass of solvent in the posolyte and negolyte, respectively, and M_0 is the molar mass of the solvent.

Similarly, the molar concentrations can be expressed in terms of the amount of species as

$$c_{\alpha,\pm} = \frac{n_{\alpha,\pm}}{V_{\pm}} = \frac{n_{\alpha,\pm}}{\sum_{\beta=0}^{N} V_{m,\beta,\pm} n_{\beta,\pm}}, \tag{4}$$

where $V_{\pm}$ is the total electrolyte volume of the posolyte and negolyte, respectively, and $V_{m,\beta,\pm}$ denotes the partial molar volume of constituent $\beta_{\pm}$.

4 Redox Reactions

Let us consider the unimolecular one-electron transfer redox reactions

$$\mathscr{M}_{\mathrm{ox},-} + e^- \underset{\text{discharge}}{\overset{\text{charge}}{\rightleftharpoons}} \mathscr{M}_{\mathrm{red},-}, \tag{5}$$

$$\mathscr{M}_{\mathrm{red},+} \underset{\text{discharge}}{\overset{\text{charge}}{\rightleftharpoons}} \mathscr{M}_{\mathrm{ox},+} + e^-, \tag{6}$$

where $\mathscr{M}_{\mathrm{red},-}$ and $\mathscr{M}_{\mathrm{ox},-}$ denote the reduced and oxidized form of a species in the negative electrode. Analogously, $\mathscr{M}_{\mathrm{red},+}$ and $\mathscr{M}_{\mathrm{ox},+}$ denote the reduced and oxidized form of a species in the positive electrode.

Alternatively, the redox reactions can be formulated as

$$\nu_{\mathrm{ox},\pm} \mathscr{M}_{\mathrm{ox},\pm} + \nu_{\mathrm{red},\pm} \mathscr{M}_{\mathrm{red},-} \rightleftharpoons e^-, \tag{7}$$

with the stoichiometric coefficients $\nu_{\mathrm{ox},\pm} = -1$ and $\nu_{\mathrm{red},\pm} = 1$.

The redox reactions (5) and (6) can be written equivalently in terms of neutral components as

$$\mathscr{S}_{\mathrm{ox},-} + e^- \underset{\text{discharge}}{\overset{\text{charge}}{\rightleftharpoons}} \mathscr{S}_{\mathrm{red},-} + a_{\alpha^\star} \mathscr{M}_{\alpha^\star}, \tag{8}$$

$$\mathscr{S}_{\mathrm{red},+} + a_{\alpha^\star} \mathscr{M}_{\alpha^\star} \underset{\text{discharge}}{\overset{\text{charge}}{\rightleftharpoons}} \mathscr{S}_{\mathrm{ox},+} + e^-, \tag{9}$$

where $\mathscr{M}_{\alpha^\star}$ denotes as before an ionic species being transferred through the membrane to satisfy the charge neutrality in the electrode compartments and $a_{\alpha^\star}$ is a stoichiometric coefficient. Similarly, as above, $\mathscr{S}_{\mathrm{red},-}$ and $\mathscr{S}_{\mathrm{ox},-}$ denote the reduced and oxidized form of a neutral component in the negolyte, respectively. Analogously, $\mathscr{S}_{\mathrm{red},+}$ and $\mathscr{S}_{\mathrm{ox},+}$ denote the reduced and oxidized form of a neutral component in the posolyte. The neutral components in the redox reaction are related to the in general charged species by the dissociation reactions (1).

Let $z_{\alpha^\star}$ denote the charge number of species $\mathscr{M}_{\alpha^\star}$. For the above one-electron transfer redox reactions to conserve the total charge, we must have $|z_{\alpha^\star}| = 1$ and

$$a_{\alpha^\star} = -z_{\alpha^\star}. \tag{10}$$

5 The TEMPTMA/Paraquat Electrolyte System

The aqueous organic TEMPO/Paraquat system, introduced by Janoschka et al. [8], has been commercialized in the start-up Jena Batteries GmbH (founded at Jena University), which is part of the SONAR and FlowCamp consortia.

The catholyte material is obtained by free radical copolymerization of a TEMPO radical (a redox-active polymer) and an amine. The anolyte material is obtained via copolymerization of 4-vinylbenzyl chloride (a viologen derivative) with an amine (see [8] for more details on the process).

TEMPTMA-Chloride salt (TCl) is used as the electroactive catholyte material. Paraquat dichloride, also called methyl viologen dichloride ($\mathrm{MVCl_2}$), serves as the anolyte. Both salts are dissolved in ionized water.

Fig. 2 shows a graphical representation of the half-cell redox reaction of the chemical system.

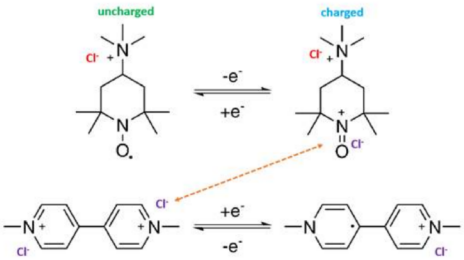

Figure 2: Reduced and oxidized forms of TEMPTMA (above) and Paraquat.

Denoting the TEMPTMA species by T and the Paraquat species by MV, we can

write the half-cell redox reactions as

$$\mathrm{MV^{2+}Cl_2^-} + e^- \underset{\text{discharge}}{\overset{\text{charge}}{\rightleftharpoons}} \mathrm{MV^+Cl^-} + \mathrm{Cl^-}, \tag{11}$$

$$\mathrm{T^+Cl^-} + \mathrm{Cl^-} \underset{\text{discharge}}{\overset{\text{charge}}{\rightleftharpoons}} \mathrm{T^{2+}Cl_2^-} + e^-. \tag{12}$$

A comparison with the more general redox reactions (8) and (9) shows that for the given chemical system $\mathscr{S}_{\mathrm{red},-} = \mathrm{MVCl}$, $\mathscr{S}_{\mathrm{ox},-} = \mathrm{MVCl_2}$, $\mathscr{S}_{\mathrm{red},+} = \mathrm{TCl}$, $\mathscr{S}_{\mathrm{ox},+} = \mathrm{TCl_2}$, as well as $\mathscr{M}_{\alpha^\star} = \mathrm{Cl^-}$ and $a_\alpha^\star = 1$.

6 Capacity and State of Charge

6.1 Ideal capacity

The ideal battery capacity is defined as the theoretical maximum amount of charge that can be extracted from the electrolytes. It is therefore proportional to the quantity of active material in the reservoirs times the number of electrons exchanged in the chemical reaction.

Assuming single-electron charge transfer reactions, the theoretical capacity of the battery at time t is given by

$$Q(t) = F \min(n_{\mathrm{red},-}(t),\, n_{\mathrm{ox},+}(t)). \tag{13}$$

6.2 State of Charge

The state of charge (SoC) of a battery is defined as the available amount of charge relative to the theoretical maximal capacity, so that $\mathrm{SoC} = 100\%$ refers to a fully charged battery and $\mathrm{SoC} = 0\%$ refers to a fully discharged battery, respectively. In terms of capacity, it is given by the ratio

$$\mathrm{SoC}(t) = \frac{Q(t)}{Q_{\max}}, \tag{14}$$

where $Q_{\max}$ denotes the theoretical maximal capacity.

Fundamentally, charging and discharging a battery results in the transfer of electrons through an external electric circuit. Due to macroscopic electroneutrality, the transfer of electrons must be balanced by the transfer of charged species through the membrane.

As such, the rate of formation (or consumption) of the active species is directly proportional to the total current, I, where we use the convention that for a discharging current $I < 0$ and for a charging current $I > 0$. The rate of change in the total number of moles is then given by

$$\frac{dn_{\mathrm{red},\pm}}{dt} = \mp\frac{I}{F}, \quad \frac{dn_{\mathrm{ox},\pm}}{dt} = \pm\frac{I}{F}. \tag{15}$$

Similarly, the total change in capacity over the time interval $[t_0, t_1]$ due to a time-dependent current, $I = I(t)$, is given by

$$Q(t) = Q_0 + \int_{t_0}^{t_1} I(t)\,dt = Q_0 + \Delta Q, \tag{16}$$

where $Q_0 = Q(t = t_0)$ denotes the capacity at $t = t_0$. The change in capacity, ΔQ, is related to changes in the number of constituents, $\Delta n_{\alpha,\pm} = n_{\alpha,\pm}(t = t_1) - n_{\alpha,\pm}(t = t_0)$, as

$$\Delta Q = \mp F \Delta n_{\mathrm{red},\pm} = \pm F \Delta n_{\mathrm{ox},\pm}. \tag{17}$$

Analogously, using the definition of the state of charge, the change in SoC is given by

$$\mathrm{SoC}(t) = \frac{Q_0}{Q_{\max}} + \frac{\Delta Q}{Q_{\max}} = \mathrm{SoC}_0 + \frac{\Delta Q}{Q_{\max}}, \tag{18}$$

where $\mathrm{SoC}_0 = \mathrm{SoC}(t = t_0)$. As such, we find that $n_{\alpha,\pm}$ are linear functions of the state of charge.

7 Initial Condition

The initial condition is given by the total electrolyte volume $V_\pm$ and the molar concentrations $c_{\mathrm{ox},-}$ and $c_{\mathrm{red},+}$ of the dissolved electroactive species in the negolyte and posolyte, respectively.

The molar concentrations satisfy the relation

$$c_{\alpha,\pm} = \frac{n_{\alpha,\pm}}{\sum_\alpha V_{m,\alpha,\pm} n_{\alpha,\pm}}. \tag{19}$$

Here we approximate the molar volume of the solvent by

$$V_{m,0,\pm} = \frac{M_0}{\rho^\star_{0,\pm}}, \tag{20}$$

where $\rho^\star_{0,\pm}$ is the mass density of the pure solvent and assume equal molar volumes of the solute species within the negolyte and posolyte ($V_{m,1,+} = V_{m,2,+}, \ldots$ and $V_{m,1,-} = V_{m,2,-}, \ldots$).

Finally, the sum over the partial mass densities satisfies

$$\rho_\pm = \sum_\alpha \rho_{\alpha,\pm} = \sum_\alpha c_{\alpha,\pm} M_{\alpha,\pm}, \tag{21}$$

where $\rho_\pm$ is a given composition-dependent mass density of the solution.

The above relations allow the approximate determination of $n_{\mathrm{red},\pm}, n_{\mathrm{ox},\pm}, n_{0,\pm}$, together with the corresponding molar volumes.

Figure 3 shows experimentally determined electrolyte mass densities for the binary TEMPTMA and Paraquat electrolyte solutions in terms of the molar concentration, together with linear least-square model approximations. For the discharged forms only the mass density of pure water and a single experimental value, at a higher molar concentration than shown in the plot, is used to define the linear model fit.

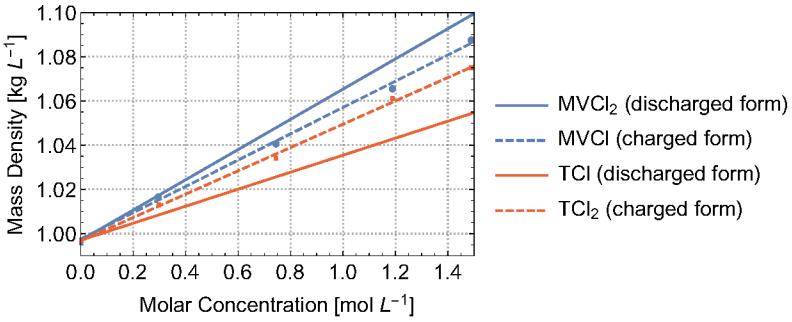

Figure 3: Mass density measurements of binary electrolyte solutions, together with a linear fit.

8 Electro-osmotic Cross-effect

The dissolution of the active materials involves the formation of a solvation shell around the charged ions. Thus, the transfer of charged particles through the membrane is generally accompanied by the transfer of solvent molecules.

As before, we assume that a single charged species $\alpha^\star$ is transferred through the membrane for charge equilibration. Let $z_{\alpha^\star}$ denote its charge number and $\kappa_{d,\alpha^\star}$ electro-osmotic drag coefficient expressed in the number of transferred solvent molecules per ionic species.

A change in the state of charge from an initial state SoC_0 to a new state SoC then leads to a change in the molar amount of solvent molecules as

$$n_{0,\pm}(\mathrm{SoC}) = n_{0,\pm}(\mathrm{SoC}_0) \mp \mathrm{sign}(z_{\alpha^\star})\kappa_{d,\alpha^\star}\frac{Q_{\max}}{F}(\mathrm{SoC} - \mathrm{SoC}_0). \tag{22}$$

Similarly, the rate of change of the amount of substance can be expressed as

$$\dot{n}_{0,\pm}(\mathrm{SoC}) = \mp \mathrm{sign}(z_{\alpha^\star})\kappa_{d,\alpha^\star} I. \tag{23}$$

The experimentally determined electro-osmotic drag coefficient $\kappa_{d,\alpha^\star} \approx 5.4$ is close to the solvation shell of Chloride ions, $\kappa_{s,\mathrm{Cl}} = 6$, see e.g. [5]. In the model the solvation shell size is used to approximate the electro-osmotic coefficient.

Figure 4a shows the change in the amount of total substance of the active species with respect to the state of charge for the TEMPTMA/Paraquat electrolyte system. The initial molar concentrations of the fully discharged electroactive material are $c_{\mathrm{MVCl}_2} = 1.49\,\mathrm{M}$ and $c_{\mathrm{TCl}} = 1.12\,\mathrm{M}$, each in an electrolyte volume

Parameter Description	Symbol	Value
Molar mass of water	M_{H_2O}	$18.02\,\mathrm{g\,mol^{-1}}$
Molar mass of chloride	M_{Cl^-}	$35.45\,\mathrm{g\,mol^{-1}}$
Molar mass of TEMPTMA-Chloride	M_{TCl}	$249.8\,\mathrm{g\,mol^{-1}}$
Molar mass of Paraquat-Dichloride	M_{MVCl_2}	$257.16\,\mathrm{g\,mol^{-1}}$

Table 2: Molar masses of the electrolyte species.

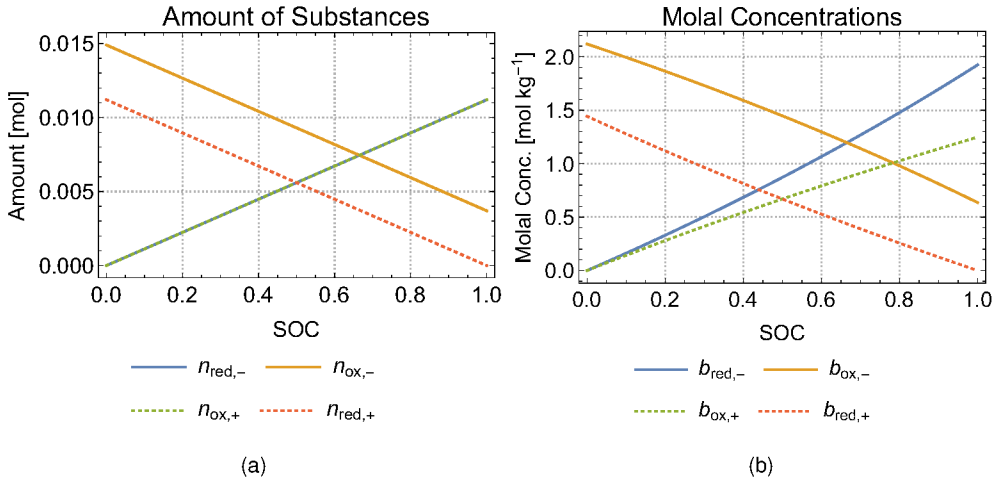

Figure 4: Amount of substance and molal concentration as a function of state of charge.

of 10 mL. The molar masses of the solvent and ions required to evaluate the total amount of substance of each species are listed in Table 2.

In contrast to the amount of substances, which are linear functions of the state of charge, the molal concentrations shown in Figure 4b are non-linear functions of the state of charge, since both the number of solvent and solute molecules are changing as a function of SoC due to electro-osmosis.

Figures 5a and 5b display the change in the total electrolyte mass and volume in the negative and positive compartments due to electro-osmosis.

9 Battery Voltage Model

In this section we present a model that allows to predict the cell voltage in terms of the species concentrations and the electric current. We proceed by first describing the equilibrium potential in terms of the species activities and continue with modeling the electrochemical reactions using the Butler-Volmer model in terms of bulk activities.

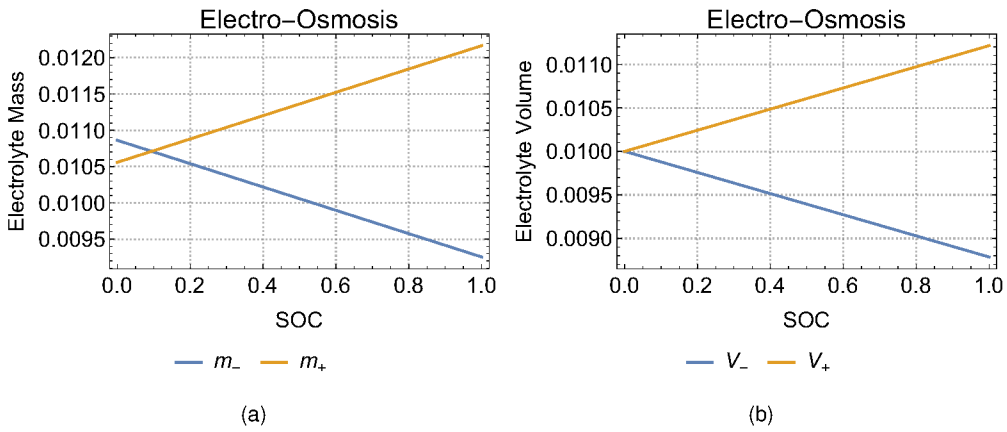

Figure 5: Total electrolyte mass and electrolyte volume as a function of state of charge.

9.1 Equilibrium Potential

In thermodynamic equilibrium, the cell voltage is determined by

$$\Delta\phi_{\mathrm{eq}} = \Delta\phi_{\mathrm{eq},+} - \Delta\phi_{\mathrm{eq},-}, \tag{24}$$

where $\Delta\phi_{\mathrm{eq},+}$ and $\Delta\phi_{\mathrm{eq},-}$ denote the reversible half-cell potentials of the positive and negative half-cell, respectively, which generally depend on the activities of the electroactive species in the electrolyte.

Let $a_{\mathrm{red},\pm}$ and $a_{\mathrm{ox},\pm}$ denote the mean chemical activities of the reduced and oxidized forms of the solutes in the positive and negative half-cells, respectively. In equilibrium, the half-cell voltages are determined by Nernst's law

$$\Delta\phi_{\mathrm{eq},\pm} = \Delta\phi^{0}_{\mathrm{eq},\pm} - \frac{RT}{F}\ln\left(\frac{a^{b}_{\mathrm{red},\pm}}{a^{b}_{\mathrm{ox},\pm}}\right), \tag{25}$$

where $a^{b}_{\mathrm{ox},\pm}$ denotes the activities in the electrolyte bulk, see e.g. Bard and Faulkner [2] on p. 91 or Kondepudi and Prigogine [9] on p. 273.

The activities can be expressed in terms of (molal) activity coefficients, $\gamma_{\alpha,\pm}$, and molal concentrations, $b_{\alpha,\pm}$, as

$$a_{\alpha,\pm} = \frac{b_{\alpha,\pm}\gamma_{\alpha,\pm}}{b^{0}}, \tag{26}$$

where b^{0} denotes an arbitrary reference molal concentration.

Relation (25) can be reformulated in terms of activity coefficients and molal concentrations as

$$\Delta\phi_{\mathrm{eq},\pm} = \Delta\phi^{0}_{\mathrm{eq},\pm} - \frac{RT}{F}\ln\left(\frac{b^{b}_{\mathrm{red},\pm}}{b^{b}_{\mathrm{ox},\pm}}\right) - \frac{RT}{F}\ln\left(\frac{\gamma^{b}_{\mathrm{red},\pm}}{\gamma^{b}_{\mathrm{ox},\pm}}\right) \tag{27}$$

$$= \Delta\phi^{0'}_{\mathrm{eq},\pm} - \frac{RT}{F}\ln\left(\frac{b^{b}_{\mathrm{red},\pm}}{b^{b}_{\mathrm{ox},\pm}}\right), \tag{28}$$

where $\Delta\phi^{0'}_{\mathrm{eq},\pm}$ denotes the formal potential given by

$$\Delta\phi^{0'}_{\mathrm{eq},\pm} = \Delta\phi^{0}_{\mathrm{eq},\pm} - \frac{RT}{F}\ln\left(\frac{\gamma^{b}_{\mathrm{red},\pm}}{\gamma^{b}_{\mathrm{ox},\pm}}\right). \tag{29}$$

Note that in the limit of dilute solutions we have $\gamma^{b}_{\mathrm{ox},\pm} = 1$, such that $\Delta\phi^{0'}_{\mathrm{eq},\pm} = \Delta\phi^{0}_{\mathrm{eq},\pm}$ and the reversible potential depends on the species concentrations only.

9.2 Butler-Volmer Overpotentials

We model the electron transfer at the electrode using the semi-empirical Butler-Volmer expression

$$i_{\pm} = i_{0,\pm}\left(g_{\mathrm{red},\pm}e^{(1-\alpha_{\pm})f\eta_{\pm}} - g_{\mathrm{ox},\pm}e^{-\alpha_{\pm}f\eta_{\pm}}\right), \tag{30}$$

where $i_{\pm}$ is the current density at the electrode surface in the positive and negative electrode, respectively and $i_{0,\pm}$ denotes the exchange current density, which is given by

$$i_{0,\pm} = i_{0,\mathrm{ref},\pm}\left(\frac{a^{b}_{\mathrm{red},\pm}}{a^{b}_{\mathrm{ref},\pm}}\right)^{\alpha_{\pm}}\left(\frac{a^{b}_{\mathrm{ox},\pm}}{a^{b}_{\mathrm{ref},\pm}}\right)^{(1-\alpha_{\pm})} \quad \text{with} \quad i_{0,\mathrm{ref},\pm} = Fk_{0,\pm}a^{b}_{\mathrm{ref},\pm}a^{b}_{\mathrm{ref},\pm}, \tag{31}$$

where $k_{0,\pm}$ is a reaction constant in units of $\mathrm{m\,s^{-1}}$ and $c^{b}_{\mathrm{ref},\pm}$, $a^{b}_{\mathrm{ref},\pm}$ denote an arbitrary reference molar concentration and activity in the electrolyte bulk. These reference values can be chosen conveniently as $c^{b}_{\mathrm{ref},\pm} = 1\,\mathrm{mol\,L^{-1}}$ and $a^{b}_{\mathrm{ref},\pm} = 1$. Furthermore,

$$g_{\alpha,\pm} = \frac{a^{s}_{\alpha,\pm}}{a^{b}_{\alpha,\pm}} \tag{32}$$

describes the dependence of the forward and backward reaction rates on the local activities. The symmetry factor, $\alpha_{\pm}$, satisfies $0 \leq \alpha_{\pm} \leq 1$ and $f = F/(RT)$ denotes the inverse of the thermal voltage. Finally,

$$\eta_{\pm} = \Delta\phi_{\pm} - \Delta\phi_{\mathrm{eq},\pm} \tag{33}$$

is the electrode overpotential in the half-cells.

Butler-Volmer type expressions in terms of activity coefficients have been used in the literature, see e.g. Balasubramanian and Weber [1]. Naturally, in the dilute solution limit, the activity coefficients in the Butler-Volmer Eq. (30) can be replaced with species concentrations and the model reduces to the expression given in the classic work by Bard and Faulkner [2] on p. 99.

The surface electric current density $i_{\pm}$ is related to the total cell current I by

$$i_{-} = -\frac{I}{A_s}, \quad i_{+} = \frac{I}{A_s}, \tag{34}$$

where A_s denotes the total solid electrode surface in each of the electrode compartments. Furthermore, the surface electric current density $i_\pm$ can be related to a volumetric electric current source $s_{q,\pm}$ by

$$s_{q,\pm} = a_s \cdot i_\pm, \tag{35}$$

where $a_s = A_s/V_{el}$ is the specific electrode surface, defined as the ratio of the total electrode surface, A_s, and the electrode volume, V_{el}.

The bulk activities, $a^b_{\alpha,\pm}$, are related to the surface activities, $a^s_{\alpha,\pm}$, by

$$a^b_{\alpha,\pm} = a^s_{\alpha,\pm} + \Delta a_{\alpha,\pm}. \tag{36}$$

Analogously, we can define the difference of molalities and the activity coefficient between the bulk and surface, $\Delta b_{\alpha,\pm}$ and $\Delta\gamma_{\alpha,\pm}$, respectively, from the relations

$$b^b_{\alpha,\pm} = b^s_{\alpha,\pm} + \Delta b_{\alpha,\pm}. \tag{37}$$

$$\gamma^b_{\alpha,\pm} = \gamma^s_{\alpha,\pm} + \Delta\gamma_{\alpha,\pm}. \tag{38}$$

Using relations (36), (37), (38) we obtain

$$g_{\alpha,\pm} = \left(1 - \frac{\Delta b_{\alpha,\pm}}{b^b_{\alpha,\pm}}\right)\left(1 - \frac{\Delta\gamma_{\alpha,\pm}}{\gamma^b_{\alpha,\pm}}\right). \tag{39}$$

In the following we assume the symmetry factor in the Butler-Volmer Eq. (30) to be given by $\alpha_\pm = 1/2$. This allows to express the overpotential η^{BV} explicitly in terms of the current density as

$$\eta^{\mathrm{BV}} = \frac{2}{f}\ln\left(\frac{i_\pm + \sqrt{i_\pm^2 + 4g_{\mathrm{ox},\pm}g_{\mathrm{red},\pm}(i_{0,\pm})^2}}{2g_{\mathrm{red},\pm}i_{0,\pm}}\right). \tag{40}$$

The above Butler-Volmer overpotential can be written in dimensionless form as

$$\bar{\eta}^{\mathrm{BV}}_\pm = 2\ln\left(\frac{\bar{\imath}_\pm + \sqrt{\bar{\imath}_\pm^2 + 4g_{\mathrm{ox},\pm}g_{\mathrm{red},\pm}(\bar{\imath}_{0,\pm})^2}}{2g_{\mathrm{red},\pm}\bar{\imath}_{0,\pm}}\right) \tag{41}$$

with the dimensionless variables

$$\bar{\eta}^{\mathrm{BV}}_\pm = \frac{\eta^{\mathrm{BV}}_\pm}{V^0}, \quad \bar{\imath}_\pm = \frac{i_\pm}{i^0_\pm}, \quad \bar{\imath}_{0,\pm} = \frac{i_{0,\pm}}{i^0_\pm} \tag{42}$$

where the characteristic voltage is given by $V^0 = f^{-1}$ and $i^0_\pm$ are some reference current densities.

9.3 Ohmic Cell Resistance

The overall Ohmic losses are given by

$$\eta^{\mathrm{Ohmic}} = I \cdot R_{\mathrm{cell}} = i_{\mathrm{mem}} \cdot A_{\mathrm{mem}} \cdot R_{\mathrm{cell}}, \tag{43}$$

where R_{cell} denotes the cell resistance, which subsumes the electronic, ionic and membrane resistances, $i_{\mathrm{mem}} = I/A_{\mathrm{mem}}$ is the current density at the electrode-membrane interfaces and $A_{\mathrm{mem}} = L_h L_w$ denotes the membrane area.

9.4 Discussion

Summarizing, the total cell potential is given by

$$\Delta\phi_{\text{cell}} = \Delta\phi_{\text{eq},+} - \Delta\phi_{\text{eq},-} + \eta_{+}^{\text{BV}} - \eta_{-}^{\text{BV}} + \eta^{\text{Ohmic}}, \tag{44}$$

with the half-cell potentials

$$\Delta\phi_{\text{eq},\pm} = \Delta\phi_{\text{eq},\pm}^{0'} - \frac{RT}{F} \ln\left(\frac{b_{\text{red},\pm}^{b}}{b_{\text{ox},\pm}^{b}}\right). \tag{45}$$

So far we have not specified how the surface concentrations are related to the bulk concentrations for a given electric current density. In Section 10.1 we discuss a transport model for the electrolyte in the boundary layer.

10 Modelling of Mass Transfer in Porous Electrode

Let us consider the flow of electrolyte through a porous carbon fiber electrode. The assumption of negligible concentration variations in the electrolyte bulk allows to simplify the transport problem and focus on the transport of species through the boundary layer forming around the carbon fibers. The solution to this transport problem determines the concentrations of the electroactive species at the electrode surface in terms of the electric current and bulk concentrations, which in turn allows the evaluation of the Butler-Volmer overpotential.

10.1 Transport in the Diffusion Layer

In the proximity of the electrode surface, a thin boundary layer is formed, in which steep concentration variations of the electroactive species can occur. By Faraday's law, the electric current density is balanced by a species mass flux density in the electrolyte, which is typically assumed to be dominated by diffusion in the boundary layer. As the current density is increased, the concentration of the reactant decreases at the electrode surface. In the limiting case of large electric current densities, the reactant concentration vanishes at the electrode surface and the electric current density reaches a limiting current density.

Even well before reaching the limiting current, an accurate description of the mass transport of the species through the boundary layer is important as it directly affects the so-called concentration overpotential that occurs when the electrochemical reactions become limited by slow transport processes.

The steady-state mass balance formulated in terms of species concentrations is

$$\operatorname{div}(c_\alpha \boldsymbol{v} + \boldsymbol{N}_\alpha) = 0. \tag{46}$$

In a first approximation, we neglect in the following the chemical potential gradient of the solvent and the migration flux. Furthermore, we assume the concentration variations of the solvent in the boundary layer to be negligible, so that the diffusive flux simplifies to

$$\boldsymbol{N}_\alpha = -\rho_0 D_\alpha \nabla b_\alpha = -D_\alpha \nabla c_\alpha. \tag{47}$$

Let $I_r = \{\mathrm{red}, \mathrm{ox}\}$ denote the species involved in the electrochemical reaction and I_n the non-reactive species. At the electrode surface, Γ_{el}, the continuity of the electric current yields the boundary condition

$$\frac{\nu_\alpha \, \boldsymbol{i}_\pm \cdot \boldsymbol{n}_s|_{\Gamma_{\mathrm{el}}}}{F} = \boldsymbol{N}_\alpha \cdot \boldsymbol{n}_l|_{\Gamma_{\mathrm{el}}} \quad \alpha \in I_r, \tag{48}$$

$$\boldsymbol{N}_\alpha \cdot \boldsymbol{n}_l|_{\Gamma_{\mathrm{el}}} = 0, \quad \alpha \in I_n, \tag{49}$$

where $\boldsymbol{n}_s$ is a normal vector pointing from the electrolyte into the solid electrode, $\boldsymbol{n}_l = -\boldsymbol{n}_l$ and ν_α is the stoichiometric coefficient of the redox reaction (7). The local electric current density $\boldsymbol{i}_\pm \cdot \boldsymbol{n}_s|_{\Gamma_{\mathrm{el}}}$ is related to the surface-averaged current density $i_\pm$ by

$$i_\pm = \frac{1}{A_s} \int_{\Gamma_{\mathrm{el}}} \boldsymbol{i}_\pm \cdot \boldsymbol{n}_s \, dA. \tag{50}$$

Figure 6 shows the electrode interface definitions for the example of a charging current in the positive electrode.

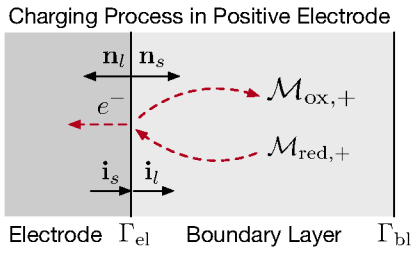

Figure 6: Illustration of the charging process in the positive electrode, together with the electrode interface definitions.

The diffusive flux at the electrode surface can be evaluated as

$$\boldsymbol{N}_\alpha \cdot \boldsymbol{n}_l|_{\Gamma_{\mathrm{el}}} = -\rho_0 \left(D_\alpha \nabla b_\alpha\right) \cdot \boldsymbol{n}_l|_{\Gamma_{\mathrm{el}}} = -k_{m,\alpha} \Delta c_\alpha \cdot \boldsymbol{n}_l|_{\Gamma_{\mathrm{el}}}, \tag{51}$$

where $k_{m,\alpha}$ denotes the convective mass transfer coefficient in units of $\mathrm{m\,s^{-1}}$ and $\Delta c_\alpha = c^b - c^s$ is the concentration difference between the bulk and the electrode surface.

10.1.1 Limiting Current

Let us consider a charging current in the positive electrode. Under the limiting current condition, the surface concentration of the species being consumed by

the electrochemical reaction depletes, so that

$$c^s_{\mathrm{red},+}\big|_{\Gamma_{\mathrm{el}}} = 0 \tag{52}$$

and the boundary condition simplifies to

$$-\rho_{0,+} D^{\gamma}_{\mathrm{red},+} \nabla b_{\mathrm{red},+} \cdot \boldsymbol{n}_l \Big|_{\Gamma_{\mathrm{el}}} = \frac{\nu_{\mathrm{red},+}\, \boldsymbol{i}_+ \cdot \boldsymbol{n}_s|_{\Gamma_{\mathrm{el}}}}{F}, \tag{53}$$

such that the limiting current is given by

$$i_{\mathrm{lim},+} = \frac{-\rho_{0,+} F D_{\mathrm{red},+} \nabla b_{\mathrm{red},+} \cdot \boldsymbol{n}_l|_{\Gamma_{\mathrm{el}}}}{\nu_{\mathrm{red},+}}. \tag{54}$$

10.1.2 Nondimensionalization

Introducing the nondimensional parameters

$$\begin{aligned} \bar{\boldsymbol{x}} &= \frac{\boldsymbol{x}}{l^0}, \quad \bar{b}_\alpha = \frac{b_\alpha}{b^0}, \quad \bar{c}_\alpha = \frac{c_\alpha}{c^0}, \quad \bar{\rho}_0 = \frac{\rho_0}{\rho^0}, \\ \bar{\boldsymbol{\imath}} &= \frac{\boldsymbol{i}}{i^0_{\mathrm{lim}}}, \quad \bar{\phi} = f\phi, \quad \bar{\boldsymbol{N}}_\alpha = \frac{\boldsymbol{N}_\alpha l^0}{\rho^0 b^0 D^0}, \end{aligned} \tag{55}$$

with the characteristic dimensional scales

$$b^0 = \frac{1}{M_0}, \quad c^0 = \rho^0 b^0, \quad \phi^0 = \frac{1}{f} \tag{56}$$

and the characteristic limiting current density

$$i^0_{\mathrm{lim}} = \frac{F D^0 c^0}{l^0} = \frac{F D^0 \rho^0 b^0}{l^0} \tag{57}$$

allows to write the boundary condition in dimensionless form as

$$\bar{\boldsymbol{N}}_\alpha \cdot \boldsymbol{n}_l\big|_{\Gamma_{\mathrm{el}}} = -\bar{\rho}_0 \bar{D}_\alpha \bar{\nabla} \bar{b}_\alpha \cdot \boldsymbol{n}_l\big|_{\Gamma_{\mathrm{el}}} = \mathrm{Sh}_\alpha \Delta \bar{c}_\alpha = \nu_\alpha \bar{\imath}, \tag{58}$$

where $\bar{\imath} = \bar{\boldsymbol{\imath}} \cdot \boldsymbol{n}_s|_{\Gamma_{\mathrm{el}}}$ and the Sherwood number, Sh, is given by

$$\mathrm{Sh}_\alpha = \frac{k_{m,\alpha}}{D^0/l^0}. \tag{59}$$

The boundary conditions are given by

$$\bar{\boldsymbol{N}}_\alpha \cdot \boldsymbol{n}_l\big|_{\Gamma_{\mathrm{el}}} = -\bar{\rho}_0 \bar{D}_\alpha \bar{\nabla} \bar{b}_\alpha \cdot \boldsymbol{n}_l\big|_{\Gamma_{\mathrm{el}}} = \mathrm{Sh}_\alpha \Delta \bar{c}_\alpha = \nu_\alpha \bar{\imath}, \tag{60}$$

$$\bar{b}_\alpha\big|_{\Gamma_{\mathrm{bl}}} = \bar{b}^b_\alpha, \tag{61}$$

where Γ_{bl} denotes the interface between the boundary layer and the bulk layer. The last expression allows to write the molar and molal concentration difference in terms of the dimensionless current as

$$\Delta \bar{c}_\alpha = \Delta \bar{b}_\alpha = \frac{\bar{\imath} \nu_\alpha}{\mathrm{Sh}_\alpha}. \tag{62}$$

The Sherwood number is typically expressed in terms of experimentally determined empirical relationships, see e.g. [3, 4, 11, 13].

Here we assume the mass transfer coefficient to satisfy

$$k_m = a_m v_s^{b_m}, \tag{63}$$

where v_s denotes the superficial velocity in the porous electrode and a_m, b_m are experimentally determined coefficients.

11 Model Validity

The underlying assumptions of the 0D-U-I-SoC model imply constraints on the RFB cell, such as the geometry or operating conditions, for the model to allow for accurate predictions. Here consider the implied constraints due to the modeling assumption of negligible concentration variations of the electrolyte species within the porous electrodes.

Let c_α^{in} and c_α^{out} denote the molar concentrations of species α at the electrode inflow and outflow boundaries. For macroscopic spatial concentration variations of species α within the porous electrodes to be negligible we require

$$|c_\alpha^{in} - c_\alpha^{out}| \ll c_\alpha^0, \tag{64}$$

where c_α^0 denotes a reference concentration, which we take as the spatial average molar concentration of species α. As shown in [12], this is equivalent to requiring the nondimensional parameter

$$\Lambda_{c_\alpha} \equiv \frac{|c_\alpha^{in} - c_\alpha^{out}|}{c_\alpha^0} = \frac{|i_{\text{mem}}| A_{\text{mem}}}{F Q_F c_\alpha^0} \tag{65}$$

to be small, i.e. $\Lambda_{c_\alpha} \ll 1$. For simplicity, we have assumed the porosity of the electrode, ε_p, to be close to unity in Eq. 65, since typical porosity values of carbon felt electrodes are in the range of $[0.8 - 1.0]$, see [7].

At large absolute current densities, the supply of reactants to the electrode surface becomes the limiting factor. The effective validity constraint is then given by the reactant species with the smallest average molar concentration in the two electrode compartments. In the following we indicate the corresponding limiting dimensionless parameter by Λ_c and the corresponding average molar concentration by c^0.

Clearly, the requirement $\Lambda_c \ll 1$ can be formulated in terms of the electric current density as

$$|i_{\text{mem}}| = \Lambda_{c_\alpha} \frac{F Q_F c_\alpha^0}{A_{\text{mem}}} \ll \frac{F Q_F c^0}{A_{\text{mem}}}, \tag{66}$$

such that the model validity requires the electric current density, $|i_{\text{mem}}|$, to be small enough, depending on the volumetric flow rate, Q_F, the average species concentration of the reactant, c^0, and the membrane area, A_{mem}.

12 Model Predictions and Experimental Validation

In this section we present an experimental validation of the 0D-U-I-SoC model for the TEMPTMA/Paraquat electrolyte system [8]. The electrode geometry of the employed laboratory test cell is described in Table 3.

Parameter Description	Symbol	Value
Electrode thickness (through-plane direction)	L_{el}	0.4 cm
Electrode width (in-plane)	L_w	2.236 cm
Electrode height (in-plane)	L_h	2.236 cm

Table 3: Electrode geometry of the test cell.

The formal half-cell potential of MV has been fitted to the experimental results of the polarization curves. Additionally, the mass transfer coefficient a_m used in the empirical mass-transfer relation $k_m = a_m v^{b_m}$ has been fitted to improve the overall agreement with the experimental data. Literature values have been taken for the specific surface area of the electrode and the reaction constants as indicated in Table 4. The initial electrolyte composition and the operating conditions of the test cell are summarized in Table 5.

Parameter Description	Symbol	Value	Source
Specific electrode surface area	a_s	$2 \times 10^5\,\mathrm{m}^{-1}$	[10]
Half-cell potential of MV	E^0_{MV}	$-0.63\,\mathrm{V}$	Fitted
Half-cell potential of TEMPTMA	E^0_{T}	$0.62\,\mathrm{V}$	Measured
Reaction constant in neg. electrode	k^0_-	$3.3 \times 10^{-5}\,\mathrm{m/s}$	[8]
Reaction constant in pos. electrode	k^0_+	$4.2 \times 10^{-5}\,\mathrm{m/s}$	[8]
Mass transport coefficient 1	a_m	$4 \times 10^{-5}\,(\mathrm{m/s})^{0.1}$	Fitted
Mass transport coefficient 2	b_m	0.9	[10]
Electro-osmotic drag	κ_{el}	6	[5]

Table 4: Chemical and material properties.

In Figure 7 we show model predictions of the cell voltage and current density for the test cell parameters introduced before and a total cell resistance of $0.286\,\mathrm{V\,A}^{-1}$. As discussed in Section 11, the assumption of negligible bulk electrolyte concentration restricts the magnitude of the current density for the model to allow for accurate predictions. We have indicated the isolines for $\Lambda_c = 10^{-2}$ and $\Lambda_c = 10^{-1}$ in the plot by a dotted and dashed curve, respectively. Generally, we expect the model validity to break down for $\Lambda_c \sim O(1)$, so that at most qualitatively correct predictions can be expected for $\Lambda_c \geq 10^{-1}$.

Thanks to the fast evaluation of the model, these plots can be generated quickly and provide a guidance to determine optimal operating conditions.

Parameter Description	Symbol	Value
Temperature	T	298.15 K
Electrolyte volume	V	10 mL
Initial molar concentration of $MV^{2+}Cl_2^-$	$c_{\mathrm{ox},-}$	1.49 mol L^{-1}
Initial molar concentration of T^+Cl^-	$c_{\mathrm{red},+}$	1.12 mol L^{-1}
Electrolyte flow rate	Q_F	16 mL/min

Table 5: Initial electrolyte concentrations and operating conditions.

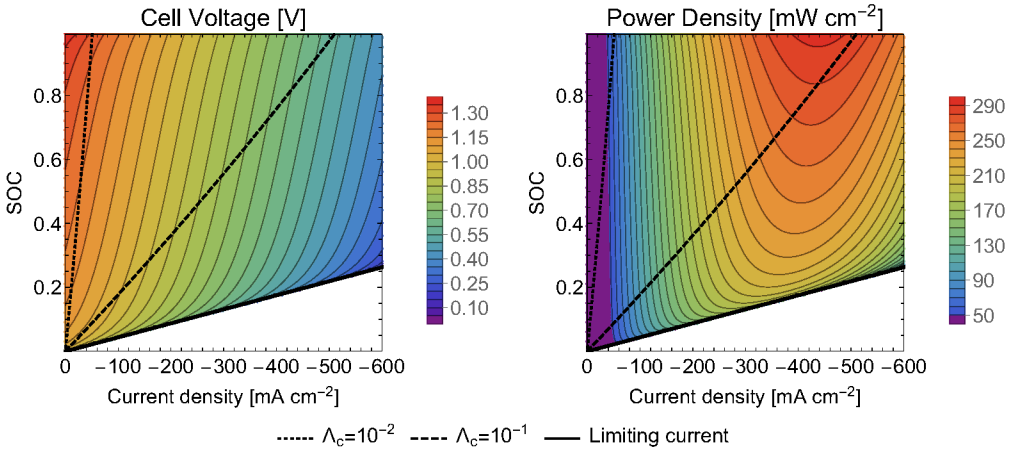

Figure 7: Polarization manifolds of the voltage (left) and power density (right) as a function of the SoC and current density.

Figure 8 shows both the measured cell voltage and power density,

$$p_{\mathrm{mem}} = \frac{I \cdot \Delta\phi_{\mathrm{cell}}}{A_{\mathrm{mem}}}, \tag{67}$$

as a function of the current density, $i_{\mathrm{mem}} = I/A_{\mathrm{mem}}$, for several polarization experiments performed at different values of the battery SoC, together with the corresponding model predictions.

The usage of a relatively small electrolyte volume results in significant changes of the SoC during the discharging periods, over which the voltage is sampled. To reflect the undesired change in SoC we evaluate the model both at the target SoC and the lowest expected SoC due to the discharging of the electrolyte. The total Ohmic cell resistance has been measured before and after the experiments by electrochemical impedance spectroscopy. The cell resistance values are given in Table 6. Similar to the change in SoC, the change in the cell resistance is considered by evaluating the model both at the lower and upper values of the measured Ohmic resistances. The lowest and highest predicted voltage and power densities for a given electric current density then define an interval of expected values. Furthermore, measurement uncertainties of the voltage are indicated by 95% confidence intervals.

The dotted and dashed vertical lines in the plots indicate the current density val-

State of Charge	Cell Resistance Before	Cell Resistance After
20%	398 mΩ	437 mΩ
50%	443 mΩ	409 mΩ
100%	409 mΩ	399 mΩ

Table 6: Measured cell resistance values before and after the polarization experiments.

ues, for which $\Lambda_c = 10^{-2}$ and $\Lambda_c = 10^{-1}$. The comparison with the experimental values shows good agreement of the model prediction up to the threshold value $\Lambda_c = 10^{-1}$, beyond which the predicted voltage and power density start to deviate more strongly and the assumption of negligible concentration variations breaks down. For a discharging current, the model validity extends to larger (negative) current densities for greater values of the SoC due to higher molar concentrations of the reactants. This allows the model to accurately predict the voltage and power density at $\mathrm{SoC} = 100\%$ up to $|i_{\mathrm{mem}}| = 500\,\mathrm{mA\,cm^{-2}}$, whereas the model prediction at $\mathrm{SoC} = 20\%$ is only accurate up to about $|i_{\mathrm{mem}}| = 115\,\mathrm{mA\,cm^{-2}}$.

Figure 9 shows the experimentally measured voltage for charge-discharge cycling experiments at constant charging and discharging currents of $80\,\mathrm{mA\,cm^{-2}}$ and $120\,\mathrm{mA\,cm^{-2}}$, together with the model predictions. The measured cell resistance values before and after the cycling experiments are $348\,\mathrm{m\Omega}$ and $360\,\mathrm{m\Omega}$, respectively. Analogous to the polarization experiment, the model is evaluated at the lower and upper cell resistance value, which allows an indication of the induced uncertainty by showing the corresponding interval of expected values.

A comparison of the model predictions with the experimental values shows that the model slightly underestimates the voltage for a charging current and overestimates the voltage for a discharging current, but allows for a qualitative good approximation of the voltage for both considered electric current densities.

13 Conclusions

The physics-based 0D-U-I-SoC model presented in this report allows for efficient single-cell performance predictions of organic RFBs. Thanks to the low computational cost of the model, parameter studies and optimizations can be readily performed, even with limited computational resources. The publicly available implementation of the model allows for a full inspection of the model and the parameters. Furthermore, being published under the open-source 3-clause BSD license allows the implementation to be used as a starting point for specific model adaptations and extensions.

The fundamental assumption of negligible spatial variations of the electrolyte bulk composition within each electrode compartment allows for a dimensionality reduction to 0D. As shown by Sharma et al. [12], this assumption is valid for typical cell geometries and operating conditions reported in the literature. How-

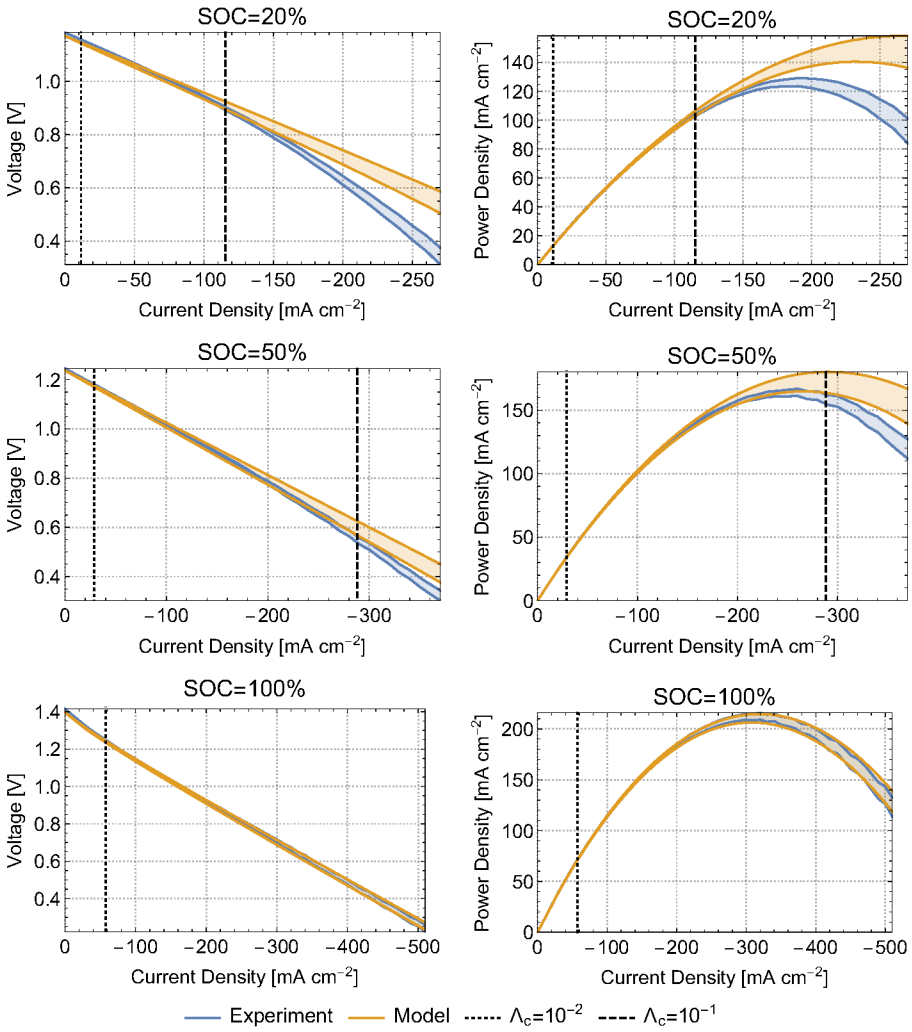

Figure 8: Measured voltage and power densities of polarization experiments, together with the model predictions.

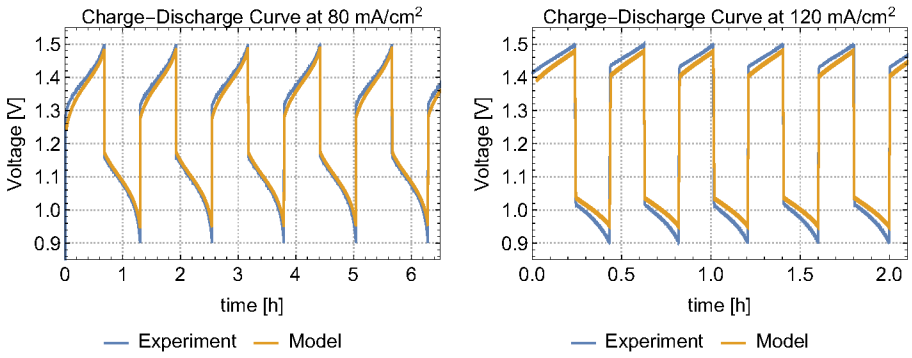

Figure 9: Charge-discharge experiments at 80 mA cm^{-2} and 120 mA cm^{-2}.

ever, it requires the electric current to be small, depending on the cell geometry, electrolyte concentration, and flow rate as discussed in Section 11.

Similar to Murthy et al. [10] we assume the symmetry coefficient in the Butler-Volmer model for single-step reactions to be given by $\alpha = 0.5$. This simplifying assumption allows for an explicit expression of the overpotential in terms of the applied current density. An extension to general symmetry coefficients is possible, but would result in an implicit formulation of the overpotential. In contrast to [10], we consider here Butler-Volmer overpotential expressions that are valid both for small and large exchange current densities.

Highly concentrated electrolyte solutions are required to achieve high energy densities, e.g. for commercial applications of RFBs. These concentrated solutions can exhibit non-ideal effects, which invalidate the often-used dilute solution hypothesis. The current model allows for the inclusion of some non-ideal effects of concentrated solutions. This is achieved by formulating the model in terms of electrolyte activities instead of concentrations, which results e.g. in standard cell potentials depending on the activity coefficient.

The experimental model validations presented in this report show that the model allows for quantitatively accurate predictions within its range of validity. As expected, the model predictions deviate from the experimental values for large absolute current densities, since the assumption of negligible concentration variations breaks down. However, also other disregarded processes, such as possible temporal temperature variations, diffusion of electroactive species through the membrane, or non-negligible side reactions could further contribute to the observed discrepancy between the model predictions and the experimentally determined voltage and power densities.

We are currently preparing a publication based on the model presented in this report for submission to a scientific journal. Furthermore, we are investigating more complex models, which allow for an extended range of validity with respect to the operating conditions. These extended models take into account macroscopic spatial variations of the electrolyte concentrations in the porous electrodes, e.g. by a spatial discretization in the direction of the convective electrolyte flow and the through-plane direction of the membrane electrode assembly.

Acknowledgments

We thank Xian Yang from JenaBatteries for performing the polarization and charge-discharge cycling experiments used for the model validation. We also thank Fritz Wernicke from JenaBatteries for his support and Diego Milian for providing mass density measurements of the TEMPTMA / Paraquat system.

References

[1] Sivagaminathan Balasubramanian and Adam Z. Weber. “Continuum, Macroscopic Modeling of Polymer-Electrolyte Fuel Cells”. In: *Physical Multiscale Modeling and Numerical Simulation of Electrochemical Devices for Energy Conversion and Storage: From Theory to Engineering to Practice*. Ed. by Alejandro A. Franco et al. London: Springer London, 2016, pp. 91–149. ISBN: 978-1-4471-5677-2. DOI: 10.1007/978-1-4471-5677-2_4 (cit. on p. 14).

[2] Allen J. Bard and Larry R. Faulkner. *Electrochemical Methods: Fundamentals and Applications, 2nd Edition*. John Wiley & Sons, Dec. 4, 2000. 862 pp. ISBN: 978-1-118-31280-3. Google Books: hQocAAAAQBAJ (cit. on pp. 13, 14).

[3] R. Carta et al. “Behaviour of a Carbon Felt Flow by Electrodes Part I: Mass Transfer Characteristics”. In: *J Appl Electrochem* 21.9 (Sept. 1991), pp. 793–798. ISSN: 0021-891X, 1572-8838. DOI: 10.1007/BF01402816 (cit. on p. 19).

[4] B. Delanghe et al. “Mass Transfer to a Carbon or Graphite Felt Electrode”. In: *Electrochimica Acta* 35.9 (Jan. 1990), pp. 1369–1376. ISSN: 00134686. DOI: 10.1016/0013-4686(90)85008-B (cit. on p. 19).

[5] Ling Ge et al. “Linking Electronic and Molecular Structure: Insight into Aqueous Chloride Solvation”. In: *Phys. Chem. Chem. Phys.* 15.31 (2013), p. 13169. ISSN: 1463-9076, 1463-9084. DOI: 10.1039/c3cp50652e (cit. on pp. 11, 20).

[6] Tino Hagemann et al. “An Aqueous All-Organic Redox-Flow Battery Employing a (2,2,6,6-Tetramethylpiperidin-1-Yl)Oxyl-Containing Polymer as Catholyte and Dimethyl Viologen Dichloride as Anolyte”. In: *Journal of Power Sources* 378 (Feb. 2018), pp. 546–554. ISSN: 03787753. DOI: 10.1016/j.jpowsour.2017.09.007 (cit. on p. 4).

[7] Thi Xuan Huong Le et al. “Carbon Felt Based-Electrodes for Energy and Environmental Applications: A Review”. In: *Carbon* 122 (Oct. 2017), pp. 564–591. ISSN: 00086223. DOI: 10.1016/j.carbon.2017.06.078 (cit. on p. 19).

[8] Tobias Janoschka et al. “An Aqueous Redox-Flow Battery with High Capacity and Power: The TEMPTMA/MV System”. In: *Angew. Chem. Int. Ed.* 55.46 (Nov. 7, 2016), pp. 14427–14430. ISSN: 14337851. DOI: 10.1002/anie.201606472 (cit. on pp. 4, 8, 20).

[9] Dilip Kondepudi and Ilya Prigogine. *Modern Thermodynamics, From Heat Engines to Dissipative Structures*. Second Edition. Wiley, 2014 (cit. on p. 13).

[10] Sri Krishna Murthy et al. “Analysis of Concentration Overpotential in an All-Vanadium Redox Flow Battery”. In: *J. Electrochem. Soc.* 165.9 (2018), A1746–A1752. ISSN: 0013-4651, 1945-7111. DOI: 10.1149/2.0681809jes (cit. on pp. 4, 6, 20, 24).

[11] D. Schmal et al. “Mass Transfer at Carbon Fibre Electrodes”. In: *J Appl Electrochem* 16.3 (May 1986), pp. 422–430. ISSN: 0021-891X, 1572-8838. DOI: 10.1007/BF01008853 (cit. on p. 19).

[12] A.K. Sharma et al. “Verified Reduction of Dimensionality for an All-Vanadium Redox Flow Battery Model”. In: *Journal of Power Sources* 279 (Apr. 2015), pp. 345–350. ISSN: 03787753. DOI: 10.1016/j.jpowsour.2015.01.019 (cit. on pp. 4, 19, 22).

[13] Xin You et al. “The Dependence of Mass Transfer Coefficient on the Electrolyte Velocity in Carbon Felt Electrodes: Determination and Validation”. In: *J. Electrochem. Soc.* 164.11 (2017), E3386–E3394. ISSN: 0013-4651, 1945-7111. DOI: 10.1149/2.0401711jes (cit. on p. 19).